Improved structural and electrical properties in native Sb2Te3/GexSb2Te3+x van der Waals superlattices due to intermixing mitigation

Cecchi, Stefano; Zallo, Eugenio; Momand, Jamo; Wang, Ruining; Kooi, Bart J.; Verheijen, Marcel A.; Calarco, Raffaella

Published in:
APL Materials

DOI:
10.1063/1.4976828

Improved structural and electrical properties in native $Sb_2Te_3/Ge_xSb_2Te_{3+x}$ van der Waals superlattices due to intermixing mitigation

Stefano Cecchi, Eugenio Zallo, Jamo Momand, Ruining Wang, Bart J. Kooi, Marcel A. Verheijen, and Raffaella Calarco

Citation: APL Materials **5**, 026107 (2017); doi: 10.1063/1.4976828
View online: http://dx.doi.org/10.1063/1.4976828
View Table of Contents: http://aip.scitation.org/toc/apm/5/2
Published by the American Institute of Physics

Improved structural and electrical properties in native $Sb_2Te_3/Ge_xSb_2Te_{3+x}$ van der Waals superlattices due to intermixing mitigation

Stefano Cecchi,[1,a] Eugenio Zallo,[1] Jamo Momand,[2] Ruining Wang,[1] Bart J. Kooi,[2] Marcel A. Verheijen,[3] and Raffaella Calarco[1]
[1]*Paul-Drude-Institut für Festkörperelektronik, Hausvogteiplatz 5-7, 10117 Berlin, Germany*
[2]*Zernike Institute for Advanced Materials, University of Groningen, Nijenborgh 4, 9747 AG Groningen, The Netherlands*
[3]*Department of Applied Physics, Eindhoven University of Technology, NL-5600 MB Eindhoven, The Netherlands*

(Received 1 December 2016; accepted 2 February 2017; published online 27 February 2017)

Superlattices made of Sb_2Te_3/GeTe phase change materials have demonstrated outstanding performance with respect to GeSbTe alloys in memory applications. Recently, epitaxial Sb_2Te_3/GeTe superlattices were found to feature $Ge_xSb_2Te_{3+x}$ blocks as a result of intermixing between constituting layers. Here we present the epitaxy and characterization of $Sb_2Te_3/Ge_xSb_2Te_{3+x}$ van der Waals superlattices, where $Ge_xSb_2Te_{3+x}$ was intentionally fabricated. X-ray diffraction, Raman spectroscopy, scanning transmission electron microscopy, and lateral electrical transport data are reported. The intrinsic 2D nature of both sublayers is found to mitigate the intermixing in the structures, significantly improving the interface sharpness and ultimately the superlattice structural and electrical properties. [http://dx.doi.org/10.1063/1.4976828]

Phase change materials (PCMs) are nowadays used as the active material for non-volatile solid-state memories, based on reversible phase transitions from amorphous to crystalline and vice versa induced by short current pulses.[1–4] The most promising materials are the alloys along the GeTe–Sb_2Te_3 pseudo-binary line. An impressive achievement has been accomplished when it was realized that PCM memory cells based on superlattices (SLs), structures made of alternating GeTe and Sb_2Te_3 layers, showed dramatically improved performance in terms of reduced switching energies with ultra-low energy consumption, enhanced write-erase cycle lifetimes, and faster switching speeds.[5–7] However, high-angle annular dark-field scanning transmission electron microscopy (HAADF-STEM) investigations carried out on molecular beam epitaxy (MBE) grown Sb_2Te_3/GeTe SLs[8] have shown that the constituting materials intermix at the interfaces, forming alternating layers of Sb_2Te_3 and natural $Ge_xSb_2Te_{3+x}$ (GST)[9] blocks with 7- to 15-atomic layers randomly distributed along the growth direction. Such phenomenon, explained in terms of the different bonding dimensionality of GeTe and Sb_2Te_3, is thermodynamically driven and therefore it cannot be easily controlled during the growth. Furthermore, the formation of GST with a different number of atomic planes results in an intrinsic loss of the vertical ordering.[10]

In the present work, we aim at verifying whether intentionally grown Sb_2Te_3/GST SLs would offer better control of the deposited layers, allowing for higher SL structural quality. Both Sb_2Te_3 and natural GST are in fact van der Waals (vdW) materials, enabling in principle their implementation in epitaxial vdW superlattice structures.[11] This would facilitate the material optimization as severe requirements to reduce intermixing would no longer be necessary. Furthermore, highly ordered SL structures would potentially enable to discriminate between the role of interface quality and SL ordering during the phase transition, unveiling the switching mechanism. Moreover, if the dispersion

[a]cecchi@pdi-berlin.de

in the GST composition along the growth direction could also be suppressed, it would be possible to engineer new SL structures by changing both the stacking and the composition of the constituting layers.

To this end, here we present the MBE growth and characterization of Sb_2Te_3/GST SLs (GST-SL) on Si(111)-($\sqrt{3} \times \sqrt{3}$)R30°-Sb passivated surfaces.[10,12,13] The repeating unit of the GST-SL investigated in this work consists of 2 quintuple layers (QLs) of Sb_2Te_3 and a $Ge_2Sb_2Te_5$ (GST225) block, giving a bilayer thickness of ~3.7 nm, as shown schematically in Figure 1(a). The GST225 features mixed occupation of Sb and Ge layers, as found in MBE grown Sb_2Te_3/GeTe SLs.[8] The number of repetitions was set to 10 and 2 QLs of Sb_2Te_3 were deposited at the end of the growth to serve as the capping layer, resulting in a 10 × [Sb_2Te_3(2 nm)/GST225(1.7 nm)]/Sb_2Te_3(2 nm) structure. Two SL samples are presented here: the first one (GST-SL A) was realized to precisely match the nominal structure, while the second (GST-SL B) features an excess of ~0.2 QL of Sb_2Te_3 meant to promote intermixing in the structure, similar to what has been found in Sb_2Te_3/GeTe SLs.[8] In order to better compare the two SL structures, the excess of Sb_2Te_3 was compensated by reducing the thickness of GST to maintain the same SL periodicity. During the growth, substrate (227.5 °C) and cell temperatures were kept constant. Flux ratios of ~0.5 and ~1.8 were used for Ge/Sb and Te/Sb, respectively.

The SLs, together with Sb_2Te_3 and GST reference samples, have been characterized by high resolution X-ray diffraction (XRD), Raman spectroscopy, and HAADF-STEM. The diffractometer used for the XRD characterization of the samples is a PANalytical X′ Pert PRO MRD system with a Ge (220) hybrid monochromator, employing a CuKα_1 (λ = 1.540598 Å) X-ray radiation. The Raman spectra were acquired in backscattering z(y,xy)-z geometry, the sample was excited with the 632.8 nm line of a He–Ne laser, and the scattered light was analyzed using a spectrometer equipped with an LN_2-cooled charge-coupled device (CCD) detector. HAADF-STEM measurements were

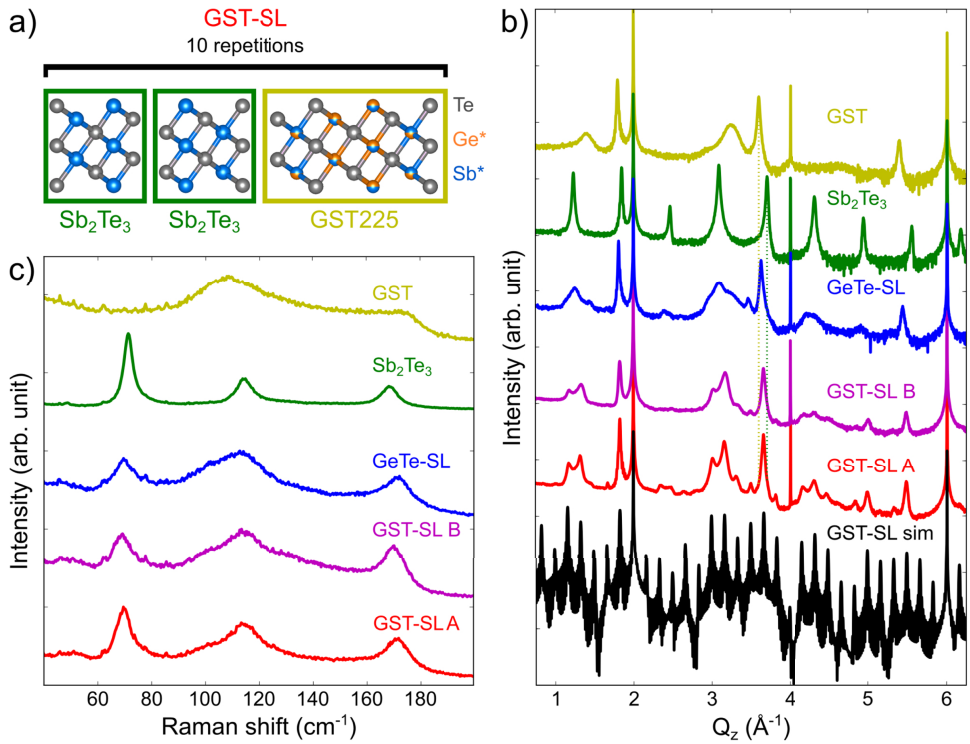

FIG. 1. (a) Schematic nominal structure of the GST-SL, where the GST block features mixed occupation (*) of Sb and Ge layers. (b) XRD radial scans of GST (green-yellow) and Sb_2Te_3 (green) reference samples, GeTe-SL (blue), GST-SL B (magenta), and GST-SL A (red). A simulated curve for the ideal GST-SL structure is shown in black. (c) Raman scattering intensity as a function of the Stokes frequency shift of GST (green-yellow) and Sb_2Te_3 (green) reference samples, GeTe-SL (blue), GST-SL B (magenta), and GST-SL A (red).

carried out using a JEOL ARM200F. Lateral electrical transport properties of both the GeTe- and GST-SL samples were studied by temperature dependent Hall measurements in the range between 4 and 300 K. In order to avoid a contribution of the substrate, the two SLs have been grown also on high-resistivity Si(111) (>5000 Ωcm). A four-contact van der Pauw configuration was realized by wire bonding the samples to the chip carriers using In droplets and Au wires. The measurements were performed applying currents and magnetic fields of 0.5 mA and 0.5 T, respectively.

The XRD radial scans of the GST-SL A and B are shown in Figure 1(b) together with those of Sb_2Te_3 and GST reference samples (red, magenta, green, and green-yellow curves, respectively). The radial scan of a 15 × [Sb_2Te_3(3 nm)/GeTe(1 nm)] SL (GeTe-SL) sample grown in analogous conditions and the simulated curve of the ideal GST-SL structure are also shown for comparison (blue and black curves, respectively). All the peaks visible in the radial scans of the GST-SLs, except the much sharper ones at ~2, 4 and 6 $Å^{-1}$ corresponding to the (111), (222), and (333) Bragg reflection of the Si substrate, are satellite peaks attributed to the SL. The position of the 0th order SL satellite peaks, the most intense in the satellite series for each diffraction order, is in between the ones of the corresponding Sb_2Te_3 and GST building blocks, as expected (see dotted line at the second order diffraction peaks). The periodicity of the SL, calculated from the satellites separation, is D_{SL} = 3.9 ± 0.4 nm, in good agreement with the nominal one. The XRD radial scan of the SL shows an intensity modulation of the satellite peaks which follows the one of the 00.3*l* peaks of Sb_2Te_3. Notably, none of the satellites is found exactly at the Q_z position of Sb_2Te_3 peaks, as generally expected in the case of SLs. The average composition of the GST reference sample, measured from the separation between the main GST peak and the corresponding 1st order vacancy layer peak,[14] is GST225. The broadening of the vacancy layer peak and the smearing out of higher order peaks is related to the coexistence in the film of different GST blocks and both cubic and rhombohedral stackings.[15] The improvement of the structural quality of the GST-SLs with respect to the GeTe-SL is immediately evident when comparing the diffraction curves: less and much broader satellites are present for the structure nominally featuring GeTe layers. Furthermore, there is a correspondence between the position of some features in the curve and that of Sb_2Te_3 and GST peaks,[10] which indicates that structural disorder is present in the SL and is responsible for the smearing out of the satellite series. In the XRD curve of GST-SL B, the SL features are weaker and broader compared to GST-SL A, as expected for intentionally intermixed SL structures, but nevertheless most of the satellite peaks are still present. Despite the additional disorder induced in the structure, GST-SL B is still characterized by a higher degree of vertical ordering as compared to the nominal GeTe-SL, which is a further indication that Sb_2Te_3/GST SL structures are intrinsically less prone to the intermixing of their constituting layers. This result also suggests that interface sharpness in vdW SLs can be controlled by accurately calibrating the growth of the constituting materials, ensuring each 2D layer in the SL to be terminated. The simulated XRD curve, which has been calculated for the ideal GST-SL structure based on the dynamical theory of diffraction,[16] shows that all expected satellite peaks can be resolved in the experimental curve of GST-SL A. However, the intensity profile of the satellites in the simulation does not perfectly match the experimental one across the whole Q_z range: this is mainly related to the slight difference between the periodicity of the grown and simulated SLs. SL models featuring less ideal structures would need to be implemented in order to accurately fit the experimental curves.

In Figure 1(c) the Raman scattering measurements for GST-SL A, GST-SL B, and GeTe-SL samples are shown (red, magenta, and blue curves, respectively), together with the ones measured for Sb_2Te_3 and GST reference samples (green and green-yellow curves, respectively). Each spectrum is normalized to its maximum and an offset for the intensity is added for a better comparison. For Sb_2Te_3, four sharp modes are excited at 48 ($E_g^{(1)}$), 71 ($A_{1g}^{(1)}$), 114 ($E_g^{(2)}$), and 169 ($A_{1g}^{(2)}$) cm^{-1}.[17] On the other hand, $Ge_2Sb_2Te_5$ alloy is characterized by broader features, with modes at 108 (overlap of E_g and A_1) and 172 (A_{1g}) cm^{-1}.[18–20] The spectrum of the SL clearly features a superposition of the modes present in the constituent materials.[21] The A_{1g} modes in the SLs are slightly shifted with respect to their corresponding ones in Sb_2Te_3, as found also for GeTe-SLs.[10] The broadening of the Raman modes could be attributed to the presence of structural disorder due to imperfect stacking of the SL building blocks with respect to the stoichiometric Sb_2Te_3. When comparing the Raman spectra of SL samples, the differences are rather small with GST-SLs having

sharper modes, particularly true for GST-SL A (see mode $A_{1g}^{(1)}$ at 69.5 cm^{-1}). The sharpening of Raman modes in GST-SLs is an indication that Sb_2Te_3/GST vdW SL structures lead to improved structural quality due to the mitigation of intermixing, in accordance with the HAADF-STEM characterization presented in the following paragraph. As described in the work of Wang *et al.*,[10] none of the two Raman modes of GeTe is present in the spectrum of GeTe-SL, while instead the shoulder at ~101 cm^{-1} has been assigned to the presence of GST Raman modes. This points out the intermixing of GeTe in the SL and is in accordance with the HAADF-STEM characterization, where only GST blocks were found along the stacking.[8] Such a shoulder is also evident in GST-SLs. Moreover, in the case of GST-SL B a broad feature at ~130 cm^{-1} is visible, which is at present under further investigation.

In Figure 2(a) a HAADF-STEM cross section image of the GST-SL A sample is shown. The SL structure with its constituting Sb_2Te_3 and GST blocks is clearly regular along the growth direction, which confirms indeed the higher structural quality of native vdW SL structures found by XRD analysis. With respect to GeTe-SLs,[8] the Sb_2Te_3 blocks in GST-SLs feature much sharper interfaces and less stacking faults, which is most probably a result of the mitigation of the intermixing between constituting layers, as already evidenced in the Raman scattering analysis. It is worth to stress that, when intermixing takes place during growth, the nucleation of the GST along the in-plane direction cannot be controlled. This in turn results in the formation of GST blocks with different compositions and worsens the vertical ordering of the SL. With respect to the GST reference film, in which 5-, 7-, 9-, 11-, and 13-layer vdW systems are present and follow a Gaussian distribution around the 9-layer one, as expected for the average GST225 composition,[15] the present SL contains mainly 5-, 7- and 9-layer vdW systems, and 7-layer GST blocks seem to form from 9-layer blocks in the presence of 2-atomic-plane stacking faults. Further analysis will be carried out to clarify this aspect. Figure 2(b) shows a high resolution HAADF-STEM cross section image of the GST-SL A sample, in which the nominal structure of the SL is precisely reproduced, demonstrating the high degree of structural perfection of such SLs.

In Figure 3 the GeTe- and GST-SLs resistivity as well as the carrier mobility as a function of temperature are shown (blue and red data points, respectively). The resistivity (black lines and circles), though close, is slightly higher for the GST-SL sample. Both samples are characterized by a clear metallic behavior, as Sb_2Te_3 and GST featuring at least a partial degree of vacancy ordering.[14,22] Besides the expected decrease of the mobility as the temperature increases, the GST-SL sample has a factor ~2 higher mobility compared to the GeTe-SL (gray lines and triangles). At the same time, the 3D carrier concentration, which does not change significantly as a function of temperature, is higher in the case of the GeTe-SL ($n_{GeTe\text{-}SL} = 5.91 \times 10^{20}$ cm^{-3} and $n_{GST\text{-}SL} = 2.78 \times 10^{20}$ cm^{-3} at room temperature). To interpret these results, it is worth to mention that in the presence of stacking faults the density of vacancies, and consequently of intrinsic carriers, is higher compared to the case of a perfect crystal with ordered vacancies. Moreover, such defects might act as scattering centers for carriers, reducing their mobility. It is then possible to directly correlate the electrical data with the

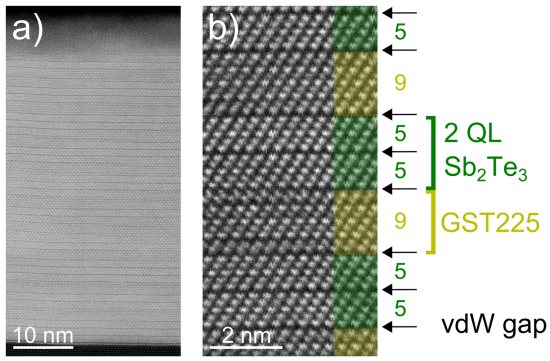

FIG. 2. HAADF-STEM cross section micrographs of GST-SL A. The image in (a) shows an overview of the whole structure, while (b) is a high resolution image with 2 Sb_2Te_3 QLs and GST225 clearly alternating, distinguished by their respective 5- and 9-layered structures.

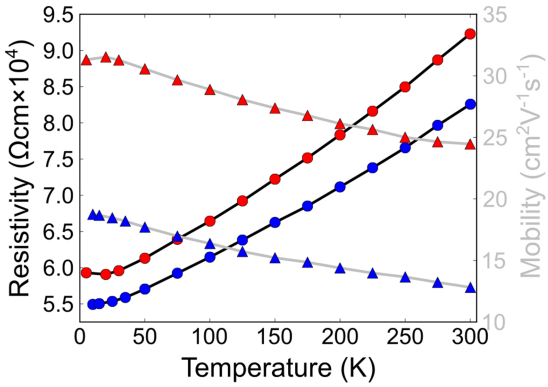

FIG. 3. Temperature dependent lateral resistivity (black lines and circles) and mobility (gray lines and triangles) of GeTe-SL (blue) and GST-SL (red) samples. The measured room temperature 3D carrier concentrations are $n_{GeTe\text{-}SL} = 5.91 \times 10^{20}$ cm^{-3} and $n_{GST\text{-}SL} = 2.78 \times 10^{20}$ cm^{-3} for GeTe-SL and GST-SL samples, respectively.

structural properties of the two SL samples: the intentional growth of GST layers in the SL results in the end in a reduced density of stacking faults, which seems to be a limiting factor to achieve higher carrier mobility.

We reported the MBE growth and characterization of Sb_2Te_3/GST van der Waals SLs, where the GST was intentionally fabricated. The investigated structure is characterized by a superior structural quality with respect to epitaxial Sb_2Te_3/GeTe SLs. In particular, the 2D nature of the constituting layers is found to mitigate the intermixing peculiar of the Sb_2Te_3/GeTe system, allowing the SL vertical ordering and interface sharpness to be precisely controlled. Notably, the Sb_2Te_3 QLs in the Sb_2Te_3/GST SLs are found to be to a great extent less defective compared to those in Sb_2Te_3/GeTe SLs, approaching the quality of Sb_2Te_3 epitaxial films. The dispersion of composition found in epitaxial GST is also remarkably reduced in the SL, where almost only 7- and 9-layer blocks are present. The interface sharpness can be controlled by accurately calibrating the growth of the SL constituting materials, ensuring each 2D layer in the SL to be terminated. Interestingly, the improved structural quality is found to give rise to a factor ∼2 increase in the lateral carrier mobility. The present results constitute a significant step forward in the control of the structural quality of Sb_2Te_3/GeTe based SL structures, potentially allowing to discriminate between the role of interface quality and SL ordering during the phase transition. Moreover, it paves the way for the engineering of new SL structures by changing both the stacking and composition of the constituting layers.

We thank S. Behnke and C. Stemmler for technical support at the MBE, M. Ramsteiner for support with Raman systems, and A. Riedel for support with the temperature dependent Hall measurement setup. O. Bierwagen is acknowledged for careful reading of the manuscript. D. Schick, J. Boschker, M. Boniardi, and A. Redaelli are acknowledged for fruitful discussion. This work was partially supported by EU within the FP7 project PASTRY (GA 317746) and partly by the Leibniz Gemeinschaft within the Leibniz Competition on a project entitled "Epitaxial phase change superlattices designed for investigation of non-thermal switching."

[1] M. Wuttig and N. Yamada, "Phase-change materials for rewriteable data storage," Nat. Mater. **6**(11), 824–832 (2007).
[2] S. Raoux, W. Wełnic, and D. Ielmini, "Phase change materials and their application to nonvolatile memories," Chem. Rev. **110**(1), 240–267 (2010).
[3] G. W. Burr, M. J. Breitwisch, M. Franceschini, D. Garetto, K. Gopalakrishnan, B. Jackson, B. Kurdi, C. Lam, L. A. Lastras, A. Padilla, B. Rajendran, S. Raoux, and R. S. Shenoy, "Phase change memory technology," J. Vac. Sci. Technol., B: Nanotechnol. Microelectron.: Mater., Process., Meas., Phenom. **28**(2), 223 (2010).
[4] A. L. Lacaita and A. Redaelli, "The race of phase change memories to nanoscale storage and applications," Microelectron. Eng. **109**, 351–356 (2013).
[5] T. C. Chong, L. P. Shi, R. Zhao, P. K. Tan, J. M. Li, H. K. Lee, X. S. Miao, A. Y. Du, and C. H. Tung, "Phase change random access memory cell with superlattice-like structure," Appl. Phys. Lett. **88**(12), 122114 (2006).
[6] R. E. Simpson, P. Fons, A. V. Kolobov, T. Fukaya, M. Krbal, T. Yagi, and J. Tominaga, "Interfacial phase-change memory," Nat. Nanotechnol. **6**(8), 501–505 (2011).

[7] T. Ohyanagi, N. Takaura, M. Tai, M. Kitamura, M. Kinoshita, K. Akita, T. Morikawa, S. Kato, M. Araidai, K. Kamiya, T. Yamamoto, and K. Shiraishi, "Charge-injection phase change memory with high-quality GeTe/Sb_2Te_3 superlattice featuring 70-μA RESET, 10-ns SET and 100M endurance cycles operations," in *2013 IEEE International Electron Devices Meeting* (IEEE, 2013), pp. 30.5.1–30.5.4.
[8] J. Momand, R. Wang, J. E. Boschker, M. A. Verheijen, R. Calarco, and B. J. Kooi, "Interface formation of two- and three-dimensionally bonded materials in the case of GeTe–Sb_2Te_3 superlattices," Nanoscale **7**(45), 19136–19143 (2015).
[9] B. J. Kooi and J. T. M. De Hosson, "Electron diffraction and high-resolution transmission electron microscopy of the high temperature crystal structures of $Ge_xSb_2Te_{3+x}$ (x = 1,2,3) phase change material," J. Appl. Phys. **92**(7), 3584 (2002).
[10] R. Wang, V. Bragaglia, J. E. Boschker, and R. Calarco, "Intermixing during epitaxial growth of van der Waals bonded nominal GeTe/Sb_2Te_3 superlattices," Cryst. Growth Des. **16**(7), 3596–3601 (2016).
[11] N. Lu, H. Guo, L. Wang, X. Wu, and X. C. Zeng, "van der Waals trilayers and superlattices: Modification of electronic structures of MoS_2 by intercalation," Nanoscale **6**, 4566–4571 (2014).
[12] J. E. Boschker, J. Momand, V. Bragaglia, R. Wang, K. Perumal, A. Giussani, B. J. Kooi, H. Riechert, and R. Calarco, "Surface reconstruction-induced coincidence lattice formation between two-dimensionally bonded materials and a three-dimensionally bonded substrate," Nano Lett. **14**(6), 3534–3538 (2014).
[13] R. Wang, J. E. Boschker, E. Bruyer, D. Di Sante, S. Picozzi, K. Perumal, A. Giussani, H. Riechert, and R. Calarco, "Toward truly single crystalline GeTe films: The relevance of the substrate surface," J. Phys. Chem. C **118**(51), 29724–29730 (2014).
[14] V. Bragaglia, F. Arciprete, W. Zhang, A. M. Mio, E. Zallo, K. Perumal, A. Giussani, S. Cecchi, J. E. Boschker, H. Riechert, S. Privitera, E. Rimini, R. Mazzarello, and R. Calarco, "Metal-Insulator transition driven by vacancy ordering in GeSbTe phase change materials," Sci. Rep. **6**, 23843 (2016).
[15] A. M. Mio, S. M. S. Privitera, V. Bragaglia, F. Arciprete, C. Bongiorno, R. Calarco, and E. Rimini, "Chemical and structural arrangement of the trigonal phase in GeSbTe thin films," Nanotechnology **28**, 65706 (2017).
[16] D. Schick, A. Bojahr, M. Herzog, R. Shayduk, C. Von Korff Schmising, and M. Bargheer, "UDKM1DSIM-A simulation toolkit for 1D ultrafast dynamics in condensed matter," Comput. Phys. Commun. **185**(2), 651–660 (2014).
[17] G. C. Sosso, S. Caravati, and M. Bernasconi, "Vibrational properties of crystalline Sb_2Te_3 from first principles," J. Phys.: Condens. Matter **21**(9), 95410 (2009).
[18] G. C. Sosso, S. Caravati, R. Mazzarello, and M. Bernasconi, "Raman spectra of cubic and amorphous $Ge_2Sb_2Te_5$ from first principles," Phys. Rev. B **83**(13), 134201 (2011).
[19] V. Bragaglia, K. Holldack, J. E. Boschker, F. Arciprete, E. Zallo, T. Flissikowski, and R. Calarco, "Far-infrared and Raman spectroscopy investigation of phonon modes in amorphous and crystalline epitaxial GeTe-Sb_2Te_3 alloys," Sci. Rep. **6** 28560 (2016).
[20] E. Zallo, S. Cecchi, J. E. Boschker, A. M. Mio, F. Arciprete, S. Privitera, and R. Calarco, "Modulation of van der Waals epitaxy induced by strain control at the step edges" (unpublished).
[21] E. Zallo, R. Wang, V. Bragaglia, and R. Calarco, "Laser induced structural transformation in chalcogenide based superlattices," Appl. Phys. Lett. **108**(22), 221904 (2016).
[22] Y. Takagaki, A. Giussani, K. Perumal, R. Calarco, and K.-J. Friedland, "Robust topological surface states in Sb_2Te_3 layers as seen from the weak antilocalization effect," Phys. Rev. B **86**(12), 125137 (2012).